

## Article

# Effect of Nano-Silica and Sorbitol on the Properties of Chitosan-Based Composite Films

Wei Zhang <sup>1</sup>, Wentao Zhou <sup>1</sup>, Zisen Zhang <sup>2</sup>, Di Zhang <sup>2</sup>, Zhengzheng Guo <sup>1</sup>, Penggang Ren <sup>1,\*</sup>  and Fei Liu <sup>3,\*</sup>

<sup>1</sup> Faculty of Printing, Packaging Engineering and Digital Media Technology, Xi'an University of Technology, Xi'an 710048, China; zhangwei@xaut.edu.cn (W.Z.); xutwentao@163.com (W.Z.); 18829029028@163.com (Z.G.)

<sup>2</sup> School of Mechanical and Precision Instrument Engineering, Xi'an University of Technology, Xi'an 710048, China; 15797716937@163.com (D.Z.)

<sup>3</sup> School of Materials Science and Engineering, Xi'an Polytechnic University, Xi'an 710048, China

\* Correspondence: rengpg@126.com (P.R.); fayeliu@xpu.edu.cn (F.L.)

**Abstract:** Chitosan and its derivatives are widely used in food packaging, pharmaceutical, biotechnology, medical, textile, paper, agriculture, and environmental industries. However, the flexibility of chitosan films is extremely poor, which limits its relevant applications to a large extent. In this paper, chitosan/sorbitol/nano-silica (CS/sorbitol/SiO<sub>2</sub>) composite films were prepared by the casting film method using chitosan, sorbitol, Tween-80 and nano-SiO<sub>2</sub> as raw materials. The structure of the films was characterized by infrared spectroscopy, electron scanning microscopy, and X-ray diffraction analysis. The effects of sorbitol and nano-silica dosage on the mechanical properties, thermal properties and water vapor barrier properties of the composite film were investigated. The results show that with the gradual increase in sorbitol ( $\leq 75$  wt %), the elongation at the break of chitosan/sorbitol films significantly increased. When the addition of sorbitol was 75 wt %, the elongation at break of the chitosan/sorbitol composite film was 13 times higher than that of the chitosan film. Moreover, nano-SiO<sub>2</sub> can further improve the mechanical properties and thermal stability of the chitosan/sorbitol composite films. When the amount of nano-silica was 4.5 wt %, the composite film became more flexible, with a maximum elongation of 90.8% (which is 14 times that of chitosan film), and its toughness increased to 10.52 MJm<sup>-3</sup> (which is 6 times that of chitosan film). This study balances the tensile strength and elongation at break of the composite films by adding a plasticizer and nano-filler, providing a reference for the preparation of chitosan composites or their blending with other polymers, and has practical guiding significance for the industrial production of biomass plastics.

**Keywords:** biomass chitosan; sorbitol; nano-silica; tensile strength; elongation at break; thermal stability



**Citation:** Zhang, W.; Zhou, W.; Zhang, Z.; Zhang, D.; Guo, Z.; Ren, P.; Liu, F. Effect of Nano-Silica and Sorbitol on the Properties of Chitosan-Based Composite Films. *Polymers* **2023**, *15*, 4015. <https://doi.org/10.3390/polym15194015>

Academic Editor: Hiroshi Ito

Received: 5 September 2023

Revised: 2 October 2023

Accepted: 3 October 2023

Published: 7 October 2023



**Copyright:** © 2023 by the authors. Licensee MDPI, Basel, Switzerland. This article is an open access article distributed under the terms and conditions of the Creative Commons Attribution (CC BY) license (<https://creativecommons.org/licenses/by/4.0/>).

## 1. Introduction

Most of the packaging materials made of petroleum-based polymers cause serious environmental pollution owing to their non biodegradable properties [1]. Environmentally friendly bio-polymers are increasingly favored due to their biocompatibility, biodegradability, non-toxicity, antibacterial activity, good transparency, ease of processing, and reusability. These materials are usually prepared from biopolymers such as proteins, lipids, polysaccharides and resins [2]. Furthermore, since no microplastics are produced during the degradation process, these biopolymers pose no threat to human health [3,4].

Chitosan (CS) is a natural cationic polysaccharide copolymer obtained from chitin, and is one of the most abundant polysaccharides on earth [5]. Chitosan has many advantages, such as its biocompatibility and biodegradability, as well as being non-toxic, which means that it can promote wound-healing and has a certain antibacterial ability [6]. In addition, chitosan also has a good film-forming capacity, and is widely used in food packaging, pharmaceutical, and agriculture industries, as well as other fields [7]. Due to the presence of amino groups, chitosan can dissolve in a dilute acid solution with a pH

below 6.5 [8]. Therefore, acids such as acetate or lactate are often used to dissolve chitosan in the preparation of chitosan complexes [7]. Moreover, amino groups in chitosan also provide chitosan with functional properties: Electronegative amino groups absorb protons and have a positive charge, giving chitosan a variety of chemical, physical and biological properties, which is one of the reasons for its wide application [9,10].

Despite the many potential applications of chitosan films, studies have reported that unmodified pure films are fragile and brittle, which largely limits their application [2]. Therefore, it is necessary to improve the physical and mechanical properties of chitosan film. The key to preparing composite films with excellent flexibility is to destroy the intermolecular forces and improve the fluidity of the polymer molecular chains to weaken the brittleness of the material [11,12]. Plasticizers play an important role in modifying the physical and mechanical properties of composite film [13]. Adding a plasticizer to the film preparation process can reduce the friction between the polymer chains. The plasticizer molecules between the polymer chains break the hydrogen bond and separate the chains, which not only increases the flexibility of the film, but also improves the water vapor transmittance performance [14–16]. Consequently, many studies have mixed different kinds of plasticizers into composite films [17–20]. In order to address the shortcomings of chitosan films, Thakhiew et al. [17] prepared different chitosan-based composite films via three drying methods combined with four glycerol concentrations (0%, 25%, 75% and 125% *w/w* of chitosan). It was found that the drying methods and plasticizer concentration significantly affected the drying time, tensile strength, elongation at break and glass transition temperature of the films. Leceta et al. [18] prepared chitosan-based films plasticized with glycerol through casting. The films exhibited excellent barrier properties against water vapor and oxygen, and provided environmentally friendly materials for packaging applications. Mei et al. [19] investigated the effects of hydrophilic glycerol and hydrophobic perilla oil on the physicochemical, mechanical, optical and structural properties of starch–chitosan films. The results of Dayarian et al. [20] show that the chitosan and carboxymethyl chitosan films have promising applications in food packaging in terms of their water vapor and oxygen barrier properties. The combination of polyethylene glycol 400 and diethyl phthalate can improve the mechanical properties of the pectin composite films [13]. The plasticizers of 1-butyl-3-methylimidazolium chloride (BMIMCl) and lithium chloride (LiCl) increased the fluidity of the cellulose molecular chain, and caused the breaking elongation of the cellulose composite film to significantly increase [11]. Polyols have become the most-used plasticizer by virtue of their excellent plasticizing efficiency, large availability and reduced exudation, with an outstanding plasticizing effect on polysaccharide-based films.

In addition, nano-materials (nano-titanium dioxide, nano-silicon dioxide, nano-cellulose, etc.) can be added to the polymer matrix to form nano-composite materials with enhanced mechanical properties, which is also one of the common methods to improve the mechanical properties of composite films [6,21]. Nano-silica (SiO<sub>2</sub>) has good surface stability and a large specific surface area in acidic media, ideal thermal stability, resistance to microbial attack and a low cost. This can be combined with polymer compounds through chemical bonds or physical interaction, endowing polymer materials with special properties and leading to high-quality nanomaterials [22,23]. However, due to the existence of a large number of active silicon hydroxyl groups on the surface of nano-SiO<sub>2</sub> particles, the “agglomeration phenomenon” of nanomaterials easily occurs, meaning that it is unable to maximize phase enhancement [24,25]. Therefore, nano-SiO<sub>2</sub> needs to be functionalized with organic molecules and physically modified by surface activity treatment to be well-distributed in the polymer. By adding nano-silica to a poly(butylene adipate-co-terephthalate)/thermoplastic hydroxypropyl film with a high hydroxypropyl starch content, the horizontal tensile strength and vertical tensile strength of the composite film were increased to varying degrees [26]. In the study of Zhu et al. [27], nanosilica enhanced the mechanical properties of starch-based films and increased the tensile strength by 54%.

In this work, chitosan/sorbitol/SiO<sub>2</sub> composite films with different sorbitol and nano-SiO<sub>2</sub> mass ratios were successfully prepared using the casting film method. The effects

of sorbitol and nano-SiO<sub>2</sub> additions on the structure, surface morphology, mechanical properties, thermal properties and barrier properties of chitosan/sorbitol/SiO<sub>2</sub> composite films were systematically examined.

## 2. Materials and Methods

### 2.1. Materials

Chitosan (CS, average molecular weight of  $7 \times 10^5 \sim 8 \times 10^5$  g/mol and deacetylated of 90%) was purchased from Hai Lan Ji Technology Development Co., Ltd. (Hai Lan Ji Technology Development Co., Ltd., Shanghai, China). Sorbitol (analytical reagent) and Tween-80 were from Tianjin Tianli Chemical Reagent Co., Ltd. (Tianli Chemical Reagent Co., Ltd., Tianjin, China). Glacial acetic acid was provided by Fuyu Fine Chemical Co., Ltd. (Fuyu Fine Chemical Co., Ltd., Tianjin, China). Nanosilica (with an average particle size of 100 nm) was purchased from Shanghai Kaiyin Chemical Co., Ltd. (Kaiyin Chemical Co., Ltd., Shanghai, China).

#### 2.1.1. Preparation of CS/Sorbitol Composite Films

Figure 1a shows the preparation process of the chitosan/sorbitol composite films. 2% (*w/v*) chitosan powders were dissolved in 50 mL of 2% (*v/v*) acetic acid solution. A different amount (30%, 45%, 60%, and 75% *w/w*) of sorbitol was added in 2% chitosan solution and stirred at 70 °C for 30 min. After naturally cooling to room temperature, the mixed solution was poured into a PTFE mold (80 mm × 80 mm), then placed in a constant temperature and humidity box with a temperature of 50 °C and humidity of 50% for 24 h. CS<sub>30</sub>, CS<sub>45</sub>, CS<sub>60</sub> and CS<sub>75</sub> represent chitosan with the addition of 30%, 45%, 60%, and 75% (*w/w*) sorbitol, respectively.

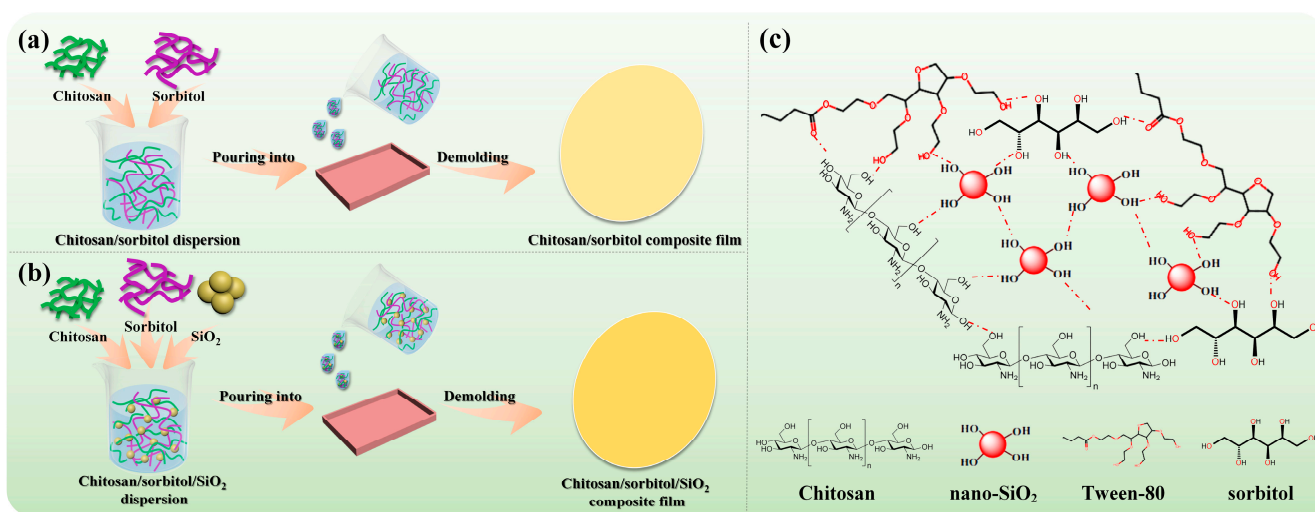


**Figure 1.** Preparation process diagram of the (a) chitosan/sorbitol composite films, and (b) chitosan/sorbitol/SiO<sub>2</sub> composite films. (c) The structural scheme of the interaction between chitosan, sorbitol, Tween-80 and nano-SiO<sub>2</sub>.

#### 2.1.2. Preparation of CS/Sorbitol/SiO<sub>2</sub> Composite Films

The preparation process of the chitosan/sorbitol/nanosilica (CS/sorbitol/SiO<sub>2</sub>) composite films is described in Figure 1b. CS<sub>60</sub> was selected for further research with 2.5%, 4.5%, and 6.5% (*w/w*) of nano-SiO<sub>2</sub> powders added to three different beakers containing 49 mL of deionized water (0.5 g Tween-80 as dispersant), respectively, and stirred with a magnetic stirrer at room temperature for 45 min. For the concentration of nano-SiO<sub>2</sub>, refer to the work of Marangoni et al. [28]. These were dispersed with ultrasonic (ultrasonic power 120 W, ultrasonic time 30 min) and magnetic stirring at room temperature for 45 min. A total of 1 mL of acetic acid solution, 2% chitosan and 60% sorbitol were

added to the dispersed nano-SiO<sub>2</sub> powders Tween solution and stirred at 70 °C for another 30 min to obtain CS/sorbitol/SiO<sub>2</sub> composite films, named CS<sub>60</sub>/SiO<sub>2</sub>-2.5, CS<sub>60</sub>/SiO<sub>2</sub>-4.5, and CS<sub>60</sub>/SiO<sub>2</sub>-6.5, respectively. Figure 1c shows the structural scheme, highlighting the interaction between chitosan, Tween-80 and SiO<sub>2</sub>.

## 2.2. Characterization

### 2.2.1. Fourier-Transform Infrared (FTIR) Spectroscopy

The samples were scanned within the wavelength range of 4000–400 cm<sup>-1</sup> using Nicolet iS50 Fourier transform infrared spectrometer, with a resolution of 2 cm<sup>-1</sup> and a scanning frequency of 32 times. The data were analyzed using Origin v2021 software (Origin Lab Corporation, Northampton, MA, USA).

### 2.2.2. X-ray Diffraction (XRD)

The crystalline structure of the composite films was analyzed using a DX-2700BH X-ray diffractometer. The tube voltage was 40 kV, the tube current was 30 mA, and the scanning rate was 10°/min. All the films were performed within the 2θ range of 5~40°, with a step size of 0.02°.

### 2.2.3. Scanning Electron Microscopy (SEM)

A scanning electron microscope (SU8000, JEOL Compact, Tokyo, Japan) was used to observe the morphology of all composite films. The films were brittlefractured by freezing with liquid nitrogen and sputtered with a gold layer. The images were observed at an accelerating voltage of 10.0 kV and current of PC40.

### 2.2.4. Mechanical Properties of the Composite Films

Mechanical properties were measured with a C610 intelligent electronic tensile testing machine according to ASTM D638 [29]. The composite films were cut into strips (8 cm × 1 cm) with a razor blade. The thickness of the sample was measured using a C640 thickness gauge at three different positions. Then, samples were tightened onto the fixture of the electronic tensile testing machine, with the initial fixture spacing and stretching speed set to 50 mm and 50 mm/min, respectively. The tensile strength (TS) and elongation at break (EAB) were calculated using Equation (1) and Equation (2), respectively:

$$TS \text{ (MPa)} = F_{\max} / S \quad (1)$$

where  $F_{\max}$  is the maximum load, and  $S$  is the cross-sectional area of the film.

$$EAB \text{ (\%)} = (L - L_0) / L_0 \times 100 \quad (2)$$

where  $L$  is the length at which the film breaks, and  $L_0$  is the initial length of the film sample.

### 2.2.5. Thermogravimetric Analysis (TG)

Thermogravimetric analysis of sample films was performed by a thermogravimetric analyzer (TG209F3 Tarsus, Selb, Germany) ranging from 30 °C to 500 °C with a heating rate of 10 °C/min. The test was conducted under a nitrogen atmosphere with a flow rate of 30 mL/min. Each sample was tested with a mass of approximately 5–10 mg.

### 2.2.6. Dynamic Mechanical Analysis (DMA)

The DMA 242E dynamic thermo-mechanical analyzer (DMA) of NETZSCH was used for the test. The experiment was conducted at a temperature range of 30~200 °C and a heating rate of 5 °C/min. The gas flow rate was 20 mL/min in nitrogen atmosphere.

### 2.2.7. Differential Scanning Calorimetry (DSC)

Differential scanning calorimetry (DSC) measurements were performed by a DSC200F3 (NETZSCH, Selb, Germany). The first heating increased from 0 °C to 200 °C and was kept

at 200 °C for 3 min to eliminate the thermal history of the material. Then, at a cooling rate of 10 °C/min, the temperature dropped to 30 °C. The second heating process increased to 200 °C with a heating rate of 10 °C/min. The thermal properties of the composite film during the second temperature rise were analyzed.

#### 2.2.8. Water Vapor Permeability (WVP)

A W3/060 water vapor permeability tester was used, with 4 cycles and an interval of 60 min. During the test, the chitosan composite films were cut into circular pieces with a diameter of 8 cm, and the thickness of the film was measured with a micrometer. Then, it was placed in a moisture permeable cup, with a temperature of 25 °C and a humidity of 50% RH for testing. The WVP was calculated using Equation (3):

$$\text{WVP}(\text{g}\cdot\text{cm}/\text{cm}^2\cdot\text{s}\cdot\text{Pa}) = (\Delta m \cdot X) / (S \cdot \Delta P \cdot t) \quad (3)$$

where  $\Delta m$  is the weight change of cup (g);  $X$  is the thickness of the film (cm);  $S$  is the effective area of the film ( $\text{cm}^2$ );  $\Delta P$  is the difference in partial water vapor pressure between the two sides of films (Pa);  $t$  is the time of the weight change (s).

#### 2.2.9. Water Contact Angle (WCA)

The WCA of the film surface was measured using a JC2000C1 contact angle measuring instrument at 25 °C. Three different positions of each film were measured; the volume of the water drop was 5  $\mu\text{L}$  and each sample was measured three times.

#### 2.2.10. Statistical Analysis

Statistical analysis was carried out using Origin v2021 software (Origin Lab Corporation, USA) and SPSS (v17.0, Chicago, IL, USA) software. All statistical data were determined with one-way analysis of variance (ANOVA) and Duncan's multiple tests using SPSS. Significant differences were defined as  $p \leq 0.05$ .

### 3. Results and Discussion

#### 3.1. Microstructural Morphology of Chitosan-Based Composite Films

##### 3.1.1. Fourier Transform Infrared (FT-IR) Spectroscopy

To investigate the structural differences between the chitosan-based composite films with and without  $\text{SiO}_2$ , IR spectra were recorded. The FTIR spectra of  $\text{CS}_{60}$  and  $\text{CS/sorbitol/SiO}_2$  composite films are shown in Figure 2a. From the FTIR spectra curve of the  $\text{CS}_{60}$  composite film, it can be seen that  $3244 \text{ cm}^{-1}$  is the hydroxyl (O-H) stretching vibration absorption peak, and the peaks at  $2921 \text{ cm}^{-1}$  and  $2882 \text{ cm}^{-1}$  correspond to the two C-H stretching vibration absorption peaks. The absorption peak of the amide II band (N-H bending vibration) is found at  $1597 \text{ cm}^{-1}$ ;  $1408 \text{ cm}^{-1}$  corresponds to the bending and deformation absorption peaks of  $=\text{CH}_2$  and  $-\text{CH}_3$ ;  $1156 \text{ cm}^{-1}$  is the C-O stretching vibration absorption peak of the  $\beta$ -glucoside bond;  $1080 \text{ cm}^{-1}$  and  $1021 \text{ cm}^{-1}$  are the two stretching vibration absorption peaks of C-O. In the fingerprint area,  $894 \text{ cm}^{-1}$  corresponds to the absorption peak of C-O stretching vibration [30,31].

From the FTIR spectra curves of  $\text{CS/sorbitol/SiO}_2$  composite films in Figure 2a, the peak value between  $3600$  and  $3000 \text{ cm}^{-1}$  was caused by the stretching vibration of the amino (N-H) and hydroxyl (-OH) groups, widening the peak value of  $3244 \text{ cm}^{-1}$ , indicating that nano- $\text{SiO}_2$  enhanced the hydrogen bond between chitosan and sorbitol and improved their compatibility [12]. In addition, the positions of absorption peaks at  $1597 \text{ cm}^{-1}$ ,  $1156 \text{ cm}^{-1}$  and  $894 \text{ cm}^{-1}$  were unchanged, indicating that amino and  $\beta$ -glucoside bonds were not involved in the reaction. The absorption peak at  $1095 \text{ cm}^{-1}$  (C-O stretching vibration on  $\text{C}_3$ ) moved toward the low wave number of  $1080 \text{ cm}^{-1}$ , and the absorption peak at the  $1027 \text{ cm}^{-1}$  wavelength (C-O stretching vibration on  $\text{C}_6$ ) moved in the low wave direction to  $1021 \text{ cm}^{-1}$  [32,33]. The movements of these two absorption peaks indicate that there was an intermolecular hydrogen bond between nano- $\text{SiO}_2$  and chitosan molecules. Moreover, an

absorption peak appeared at  $952\text{ cm}^{-1}$ , which might be the stretching vibration absorption peak of Si-OH [34]. It was indicated that nano-SiO<sub>2</sub> grows on a molecular chain skeleton of the CS<sub>60</sub> composites [23]. The functionalized nano-SiO<sub>2</sub> could be dispersed in the CS<sub>60</sub> composite film, which further improves the compatibility of chitosan and sorbitol.

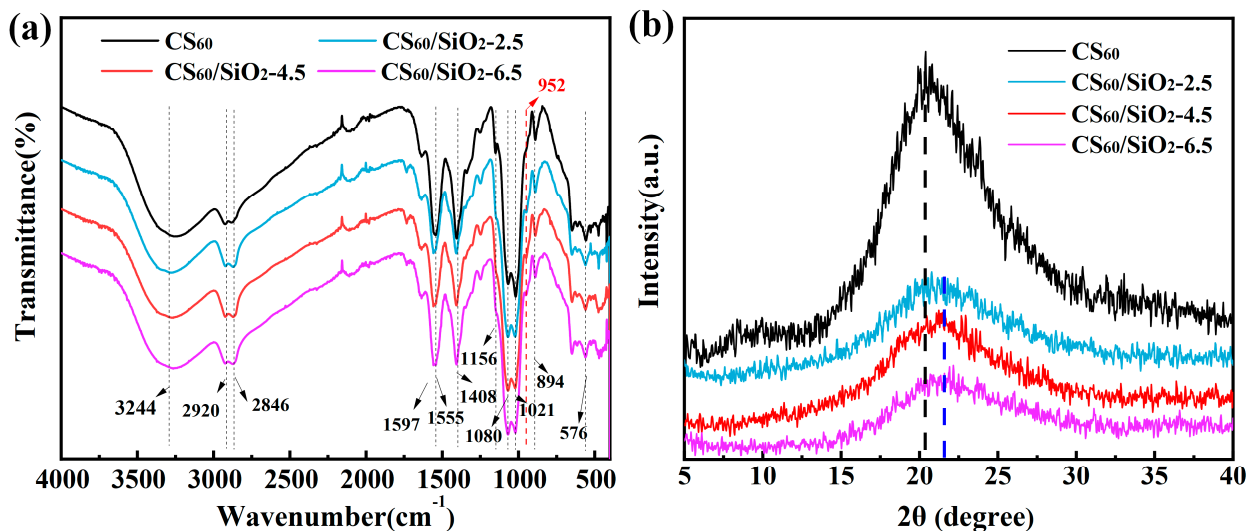


Figure 2. (a) FTIR and (b) XRD spectra of CS<sub>60</sub> and chitosan/sorbitol/SiO<sub>2</sub> composite films.

### 3.1.2. XRD Spectra Analysis

Figure 2b shows the XRD spectra of CS<sub>60</sub> and CS/sorbitol/SiO<sub>2</sub> composite films. In the CS<sub>60</sub> film at  $2\theta = 10^\circ$  and  $2\theta = 20^\circ$ , there is a wide diffraction peak, which is a typical fingerprint of the chitosan/sorbitol composite film [35]. Additionally, the diffraction peak located at  $2\theta = 10^\circ$  is recognized as the crystalline hydrate of chitosan, and the diffraction peak that appeared at  $2\theta = 20^\circ$  is assigned to the anhydrous crystallization of chitosan. Consequently, the hydrogen bonds between the molecular chains of chitosan affect the crystallization behavior of chitosan, and the molecular conformation of chitosan has a significant effect on the crystalline form of chitosan [36,37].

In the XRD spectra of CS/sorbitol/SiO<sub>2</sub> composite films, the diffraction peaks of films at  $10^\circ$  all disappeared after nano-SiO<sub>2</sub> was added. As the silicon dioxide content increased, the diffraction peak intensity at  $2\theta = 20^\circ$  significantly decreased and gradually moved towards  $2\theta = 21.7^\circ$ , indicating the less crystalline structure formed in the chitosan matrix. Nano-SiO<sub>2</sub> that undergoes surface treatment contains numerous -Si-OH groups, forming strong hydrogen bonds with chitosan molecules, which influence molecular inter-chain interactions and the movement of chitosan to a certain extent, hindering the chitosan crystallization process. Song et al. [38] and Qiao et al. [39] both reported the disappearance of the peak at  $10^\circ$  and ascribed this to the strong hydrogen bonds between new additives and chitosan; the former pointed out that this destroyed the formation of hydrogen bonds between chitosan chains, while the latter explained that it limited the movement of chitosan chains. The synergistic effect of physically modified nanoSiO<sub>2</sub> and -OH in sorbitol increases the free amino group in chitosan, which enables the double helix structure of the polysaccharide asymmetric unit of chitosan to become more unstable. The formation of an unstable architecture offers plentiful growth sites for the formation of amorphous nano-SiO<sub>2</sub> [36,40]. Based on the results of FTIR and XRD, it was determined that the inorganic phase in the prepared CS/sorbitol/SiO<sub>2</sub> films is amorphous silica [41].

### 3.1.3. SEM of Chitosan-Based Composite Films

Figure 3a shows an optical image of chitosan-based composite films. Among all films, CS has relatively high transparency and obvious folds on the surface. After adding sorbitol, the color deepens and the surface smoothness increases. The chitosan composite film

improved by functionalized nano-silica is more flexible and elastic. SEM micrographs of the surface CS and CS/sorbitol composite films are presented in Figure 3b–f. The surface of pure chitosan film is smooth, continuous and dense. Here, the addition of sorbitol did not introduce discontinuities or porous structures into the film. The films are continuous and dense, which indicates that sorbitol has good miscibility and compatibility in chitosan [2]. When adding 30% sorbitol, the microsurface of the composite film is uneven, with many wrinkles and pores appearing. This implies that the combination of chitosan and sorbitol needs to be further improved, as only a small number of hydrogen bonds are formed with sorbitol due to the inadequate hydroxyl groups [42]. The surfaces of the CS<sub>45</sub>, CS<sub>60</sub> and CS<sub>75</sub> are relatively smooth compared with CS<sub>30</sub>, without obvious gaps and pores, which indicates that chitosan and sorbitol have good intermolecular compatibility and are tightly bound. This morphology is similar to that described by previous studies [43,44]. Moreover, sorbitol molecules effectively fill the network structure between chitosan molecules, forming a continuous and uniform film, and make the structure of chitosan matrix more orderly [15,45]. Figure 3g–i show the surface morphology of the CS/sorbitol/SiO<sub>2</sub> composite films. Figure 3g shows that the surface of CS<sub>60</sub>/SiO<sub>2</sub>-2.5 is rough, with significant wrinkles and overall discontinuity. The addition of 45 mg nanoSiO<sub>2</sub> is more well-distributed in the chitosan composite film due to the presence of a large number of hydrogen bonds between nanoSiO<sub>2</sub> and the chitosan plasticizer system [46], resulting in the cross-linking network structure that formed between nanoSiO<sub>2</sub> and the chitosan polymer matrix [47]. The CS<sub>60</sub>/SiO<sub>2</sub>-6.5 composite film's surface is uneven and there are no obvious pores, but agglomeration occurs (Figure 3i). This is because the nano-SiO<sub>2</sub> content is high, and in addition to forming intermolecular hydrogen bonds with chitosan and sorbitol, there are also unbound silicon hydroxyl groups that have a large surface energy and are prone to self-aggregation [48]. SiO<sub>2</sub> is tightly deposited on the surface of chitosan, forming a non-uniform layer of silica nanoparticles [36]. A similar observation was reported by Hosseini et al. [49], who investigated the fish gelatin–chitosan nanoparticles composite and Chang et al. [50], who worked with starch–chitosan nanoparticles composites.

### 3.2. Mechanical Properties of Chitosan-Based Composite Films

Mechanical performance is an important factor in evaluating whether a film can be used for packaging, as it represents the durability and physical integrity of the film. The stress-strain curve of CS/sorbitol composite films is shown in Figure 4a. Figure 4b shows the corresponding bar charts of tensile strength and elongation at break. The tensile strength of CS film can be up to 38.91 MPa, which is the highest mechanical strength of all films, but the fracture elongation is only 5.9%, far from meeting the actual application requirements, and the toughness needs to be improved. The addition of sorbitol improved the mechanical properties of the chitosan composite film. Tensile strength, break elongation and toughness data for different chitosan-based films are shown in Table 1. The results show that with the gradual increase in sorbitol ( $\leq 75$  wt %), the elongation at break of CS/sorbitol films significantly increased. The elongation at break of the CS/sorbitol composite film was 13 times higher than that of the pure CS film when the addition of sorbitol was 75 wt %.

In addition, the tensile strength and elongation at break of CS/sorbitol composite films gradually achieve a balance with the increase in sorbitol content, and toughness reaches the highest value when chitosan–sorbitol = 1:0.6 in this research. The low viscosity of plasticizers increases the flowability of biopolymer chains, leading to film structure softening and reducing tensile strength [51]. By adding sorbitol to the chitosan film, the hydrogen bonds formed between sorbitol molecules and chitosan will interact with the intermolecular and intramolecular hydrogen bonds formed by destroying the amino and hydroxyl groups of chitosan, reducing the intermolecular force of chitosan and enhancing the mobility of molecular chains in the film (with easier intermolecular relative slip), thereby increasing the flexibility of the composite films [43,48]. When the content of sorbitol reaches 75% that of chitosan, there is still good compatibility between sorbitol and chitosan [52]. The formation of a dense membrane further increased the spatial distance of the CS molecular

chains, weakened the interchain force, increased the interchain free volume and reduced the tensile strength. However, the formation of a structurally dense film with a fracture elongation about 10 times that of the pure chitosan film fully reflects the plasticizing effect of hydroxyl (-OH) in polyol plasticizers. Therefore, the stress–strain curve exhibited the characteristics of a plastic deformation stage. An excessive dose of plasticizer can cause the plasticizer to aggregate and form small droplets, which are distributed in the network structure during the film-forming process. A stress concentration is easily formed when stretched, resulting in a serious decrease in tensile strength.

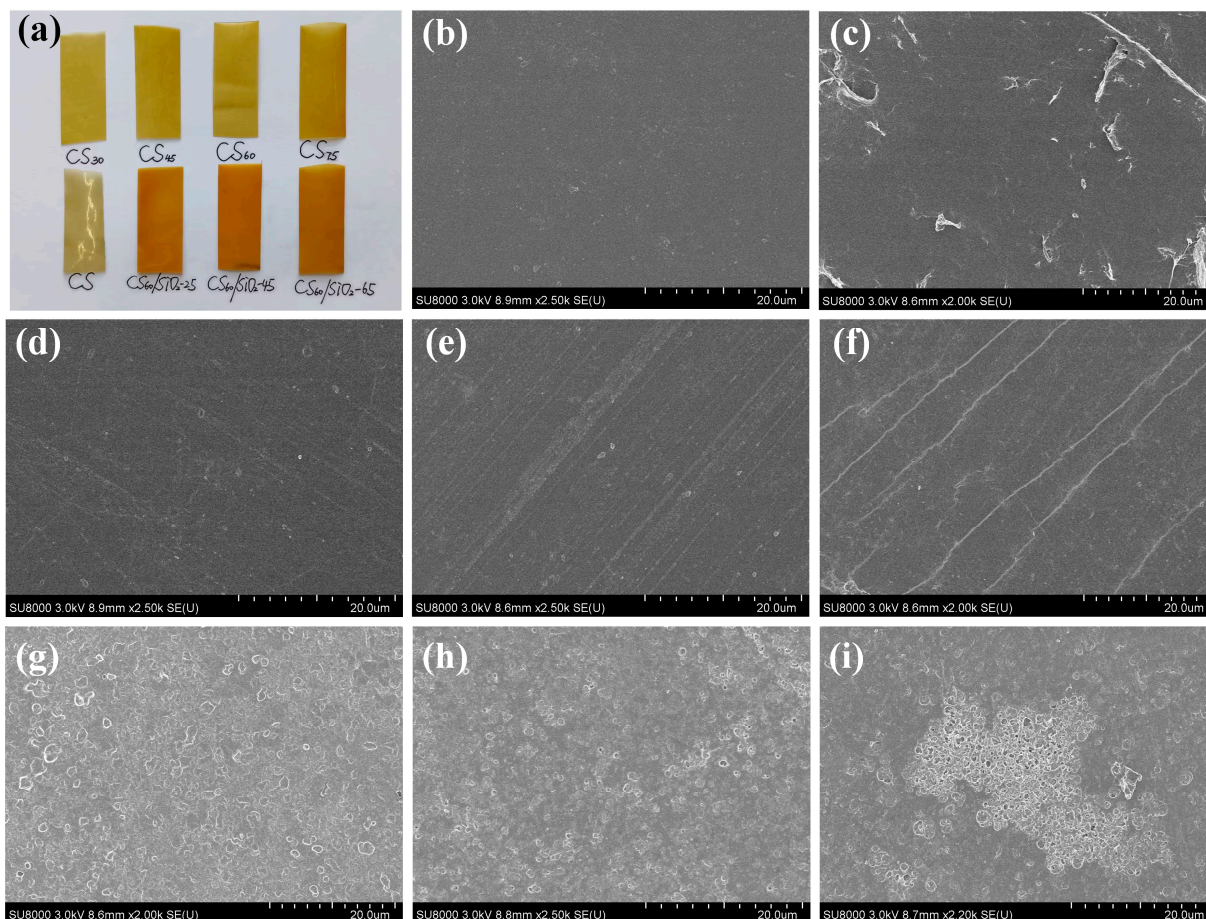


**Figure 3.** (a) Optical image of chitosan-based composite films. SEM photomicrographs of (b) CS, (c) CS<sub>30</sub>, (d) CS<sub>45</sub>, (e) CS<sub>60</sub>, (f) CS<sub>75</sub>, (g) CS<sub>60</sub>/SiO<sub>2</sub>-2.5, (h) CS<sub>60</sub>/SiO<sub>2</sub>-4.5; (i) CS<sub>60</sub>/SiO<sub>2</sub>-6.5.

**Table 1.** Tensile strength, break elongation and toughness data of different chitosan-based films. Pure chitosan (CS), chitosan with 30% (w/w) sorbitol (CS<sub>30</sub>), 45% (w/w) sorbitol (CS<sub>45</sub>), 60% (w/w) sorbitol (CS<sub>60</sub>), 75% (w/w) sorbitol (CS<sub>75</sub>). Chitosan with 0.60 g sorbitol and 2.5% (w/w) nano-SiO<sub>2</sub> (CS/SiO<sub>2</sub>-2.5), 4.5% (w/w) nano-SiO<sub>2</sub> (CS/SiO<sub>2</sub>-4.5), 6.5% (w/w) nano-SiO<sub>2</sub> (CS/SiO<sub>2</sub>-6.5), respectively.

Sample	CS	CS <sub>30</sub>	CS <sub>45</sub>	CS <sub>60</sub>	CS <sub>75</sub>	CS <sub>60</sub> /SiO <sub>2</sub> -2.5	CS <sub>60</sub> /SiO <sub>2</sub> -4.5	CS <sub>60</sub> /SiO <sub>2</sub> -6.5
TS/MPa	38.91	15.68	19.11	29.27	13.22	20.56	25.38	11.22
EAB/%	5.9	20.96	42.68	66.16	87.23	73.7	90.8	78.4
Toughness/MJm <sup>-3</sup>	1.67	2.91	4.89	8.99	4.43	6.39	10.52	3.55

Figure 4c shows the scatter plot between the toughness and tensile strength of each film. The toughness of composite films can be calculated by the area under the tensile stress–strain curve [4]. The toughness of the pure CS film is only 1.67 ± 0.13 MJm<sup>-3</sup>. It is worth noting that the film toughness obviously increased with the addition of sorbitol:

CS<sub>30</sub> ( $2.91 \pm 0.21 \text{ MJm}^{-3}$ ), CS<sub>45</sub> ( $4.89 \pm 0.26 \text{ MJm}^{-3}$ ), CS<sub>75</sub> ( $4.43 \pm 0.34 \text{ MJm}^{-3}$ ), while the toughness of the CS<sub>60</sub> film can reach  $8.99 \pm 0.4 \text{ MJm}^{-3}$ , which is more than five times that of the CS film. The toughness of the film significantly improved; the toughness was more than five times that of the pure chitosan film and superior to other films. A balance between a certain tensile strength and ideal elongation at break was also obtained. CS<sub>60</sub> has ideal tensile strength, elongation at break, and toughness, and its comprehensive mechanical properties are the best.

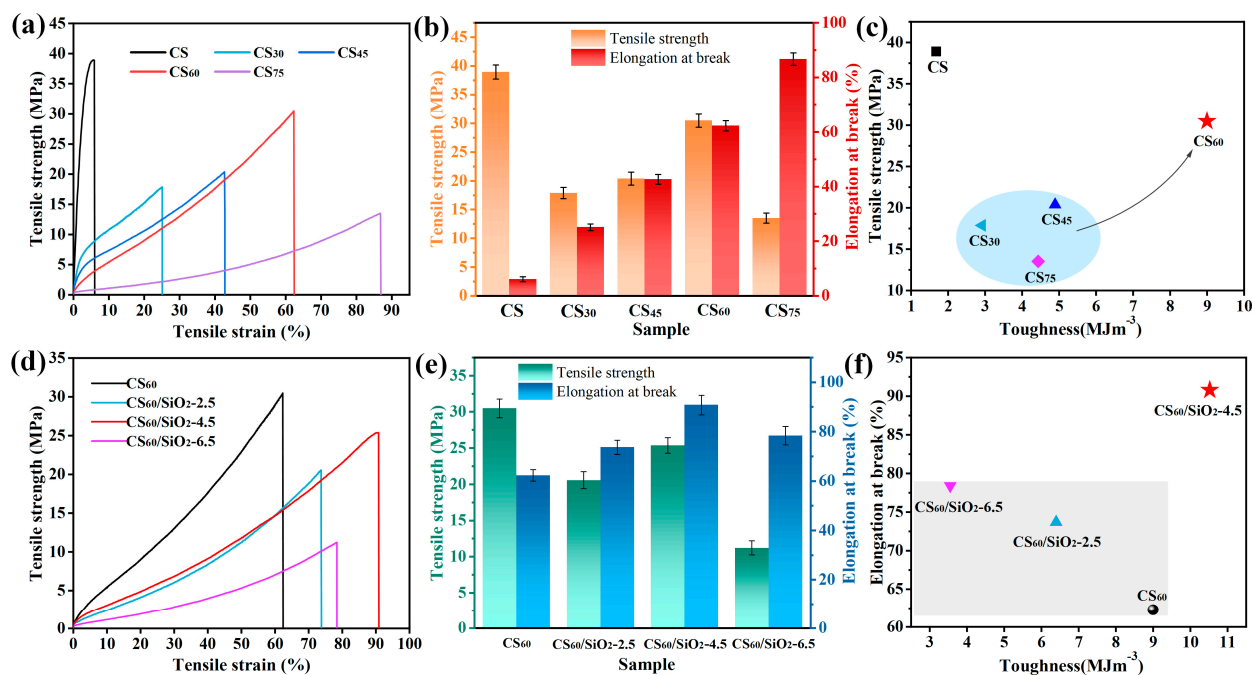


**Figure 4.** (a) Stress–strain curves, (b) bar chart of tensile strength and elongation at break, (c) toughness–tensile strength scatter plot of chitosan/sorbitol composite films. (d) Stress–strain curves, (e) bar chart of tensile strength and elongation at break, (f) toughness–elongation at break scatter plot of chitosan/SiO<sub>2</sub> composite films.

By adding nanoparticles to change the aggregation morphology of chitosan molecules, the mechanical and barrier properties of chitosan materials can be further improved. The stress–strain curve of CS/sorbitol/SiO<sub>2</sub> composite films is shown in Figure 4d. Figure 4e shows the corresponding bar charts of tensile strength and elongation at break. The data show that the addition of nano-SiO<sub>2</sub> has a significant impact on the elongation at break of chitosan composite films. When the dosage of nano-SiO<sub>2</sub> is less than 4.5%, the elongation at break of the composite film shows an increasing trend with the increase in dosage. When the amount of nano-SiO<sub>2</sub> that is added is 4.5 wt %, its tensile strength is 24.5 MPa. The elongation at break of CS<sub>60</sub>/SiO<sub>2</sub>-45 can reach up to 90.8%, which is the largest of all films and 15 times higher than that of pure chitosan films. As a surface modifier of nano-silica, Tween-80 causes the hydrogen bond force between chitosan molecules to weaken in the presence of a plasticizer [53,54], so the tensile strength of CS<sub>60</sub>/SiO<sub>2</sub> composite films is lower than that of CS<sub>60</sub>. Hou et al. [55] also improved the EAB of agar/sodium alginate films with the addition of 2.5–10% of nano-SiO<sub>2</sub>; they ascribed this enhancement to the strong interactions between nano-SiO<sub>2</sub> and the matrix via hydrogen bonding. Nano-SiO<sub>2</sub> with a large surface area tends to interact more with the hydroxyl groups and carboxylic groups of chitosan, which facilitated the transfer of stress from the matrix to the reinforcing phase via the interface. Wu et al. [56] improved the EAB of starch-based films with A<sub>g</sub> nanoparticles through the van der Waals interactions between hydroxyl groups of starch and A<sub>g</sub> nanoparticles. When the amount of SiO<sub>2</sub> exceeds 4.5%, the elongation at break decreases. The reason for this is that as the amount of nano-SiO<sub>2</sub> increases, SiO<sub>2</sub> particles

gradually aggregate and unevenly disperse, and agglomeration occurs, which disrupts the density of the film [57,58], causing defects such as “pores” to form in the composite film. During the stretching process, the sample first breaks at the “pores”. The introduction of nano-SiO<sub>2</sub> reduces the tensile strength, but the elongation at break is greatly improved, improving the toughness and processability of the composite film.

Figure 4f shows that the toughness of CS<sub>60</sub>/SiO<sub>2</sub>-4.5 ( $10.52 \pm 0.41 \text{ MJm}^{-3}$ ) is significantly better than that of the other composite films: CS<sub>60</sub>/SiO<sub>2</sub>-2.5 ( $6.39 \pm 0.28 \text{ MJm}^{-3}$ ) and CS<sub>60</sub>/SiO<sub>2</sub>-6.5 ( $3.55 \pm 0.19 \text{ MJm}^{-3}$ ). In particular, the toughness of CS<sub>60</sub>/SiO<sub>2</sub>-4.5 is six times higher than that of pure CS film, which is a 17% improvement compared to CS<sub>60</sub>. The addition of nano-silica can not only improve the compatibility of chitosan and sorbitol and improve the elongation at break of the chitosan composite film, but also further improves the film-forming performance and toughness of the chitosan composite film.

### 3.3. Thermal Property

#### 3.3.1. Thermogravimetric Analysis

Thermogravimetric analysis was used to study the weight variation of polymer films with increasing temperature. Figure 5a shows the thermogravimetric curves of CS<sub>60</sub> and CS/sorbitol/SiO<sub>2</sub> composite films. CS<sub>60</sub> without the addition of nano-silica only has two weight loss stages, while the CS/sorbitol/SiO<sub>2</sub> composite films present three weight loss stages. Stage 1: Between 30 and 200 °C, all curves show significant weight loss (about 20%), which is caused by the evaporation of free and bound water contained in the sample [30,59]. Stage 2: The significant weight loss of the CS<sub>60</sub> film at from 200 °C to 350 °C is related to complex processes such as the thermal decomposition of chitosan and sorbitol [60,61]. For CS/sorbitol/SiO<sub>2</sub> composite films, the weight loss in the temperature range of from 200 °C to 350 °C is significantly lower than that of the CS<sub>60</sub> film, indicating that interface interactions such as the hydrogen bonds formed between nano-SiO<sub>2</sub> and chitosan and sorbitol improved the thermal stability of chitosan-based composite films [62]. Furthermore, the DTG curves in Figure 5b suggest that all thermograms of CS/sorbitol/SiO<sub>2</sub> composite films exhibited similar decomposition and weight loss patterns, with a maximum degradation rate around at 275 °C, but they were significantly lower than the degradation rate of CS<sub>60</sub>. Compared to CS<sub>60</sub>, CS/sorbitol/SiO<sub>2</sub> composite films exhibit one more degradation stage in the range of 400–470 °C. The third stage: after 350 °C, the weight of CS/sorbitol/SiO<sub>2</sub> composite films continued to slowly decrease, which can be attributed to the decomposition of C-C, C-O, and C-N single bonds in chitosan, as well as the thermal degradation of Tween-80 in modified nano-SiO<sub>2</sub> micropores [36,63]. Nano-SiO<sub>2</sub> can be considered to grow on the molecular chain skeleton of the CS<sub>60</sub> composites, improving their thermal stability.

#### 3.3.2. Dynamic Mechanical Analysis and Differential Scanning Calorimetry

DMA is an effective tool for studying the relationship between polymer molecular chains, structure, and thermal-mechanical performance. Figure 5c–e depict the dynamic thermal behavior of the samples, including storage modulus, loss modulus and  $\tan \delta$ . The storage modulus decreased with the addition of SiO<sub>2</sub> 25, 45 mg, and increased with the addition of 65 mg. This suggests that the addition of SiO<sub>2</sub> may improve the storage modulus of certain content. The two peaks in  $\tan \delta$  curves correspond to two glass transition temperatures ( $T_g$ ); the first strong peak of CS<sub>60</sub> appeared at 30 °C, while the second small peak of CS<sub>60</sub> appeared at 126 °C. The addition of nano-SiO<sub>2</sub> improved the  $T_g$  of the film; the largest increase was observed in CS<sub>60</sub>/SiO<sub>2</sub>-6.5, where the first peak shifted to 62 °C. Qiao et al. [64] obtained similar results for two  $T_g$  of chitosan films solved in three acid solutions at around 55 °C and 125 °C. Ma et al. [45] also observed two  $T_g$  in a chitosan/sorbitol film, which appeared at around 15 °C and 103 °C. Liu et al. [60] reported two peaks in  $\tan \delta$  curves of chitosan film using DMA; he defined the first peak as  $\beta$ -relaxation related to the motions of the side chains, while only the second peak was associated with the  $T_g$  of chitosan films. The different chitin source, extraction methods,

molecular weights, viscosities, degrees of deacetylation and film-forming methods resulted in the divergent results in measurements of  $T_g$  in chitosan film. Previous studies reported several single- $T_g$  chitosan films including, 54–86 °C [65], 103 °C [39], 160 °C [66]. Table 2 shows the glass transition temperature of each film based on the DMA results.

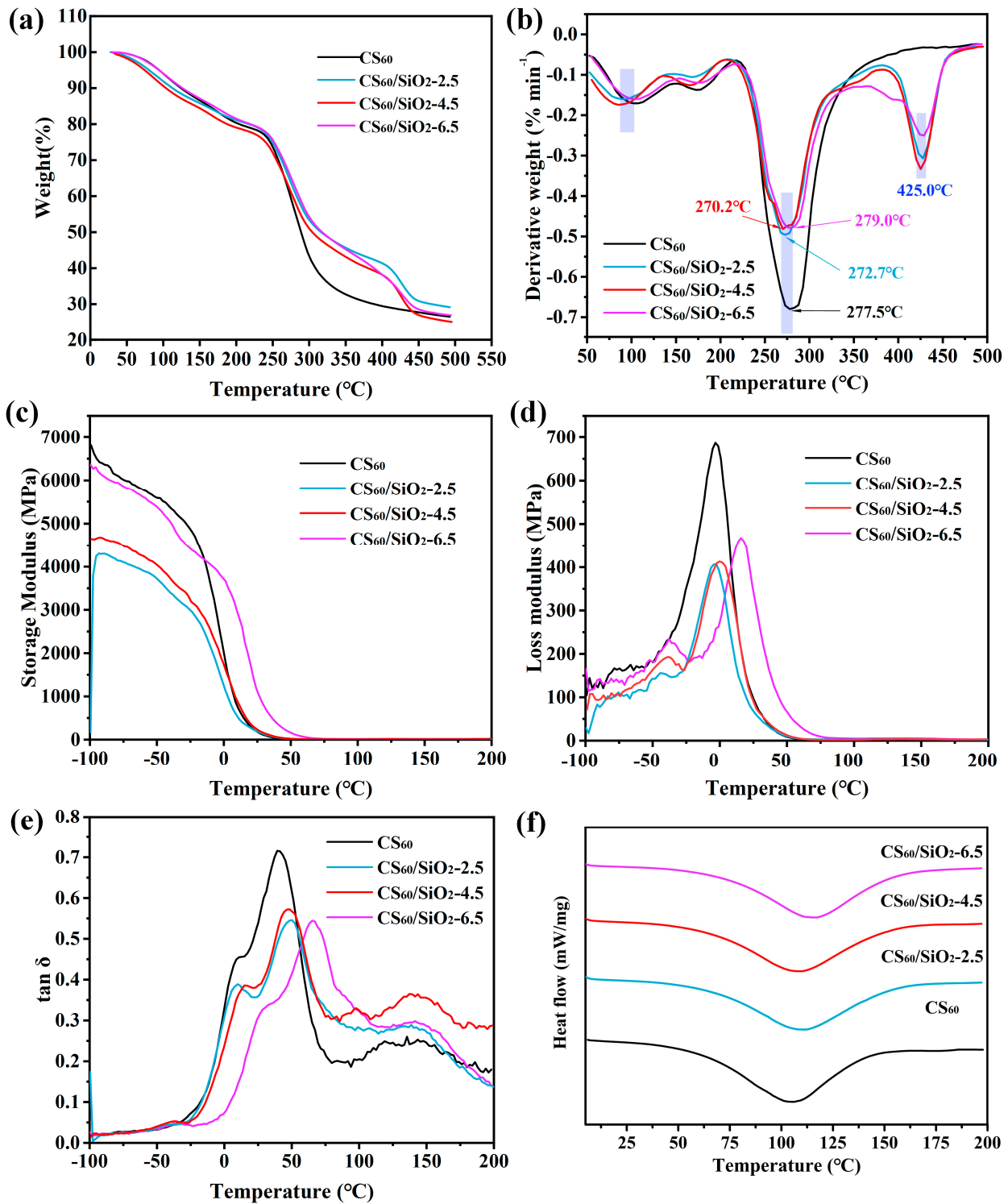


Figure 5. (a) TGA, (b) DTGA, (c) storage modulus, (d) loss modulus, (e)  $\tan \delta$ , (f) DSC curves of chitosan-based composite films.

**Table 2.** The glass transition temperature ( $T_g$ ) of samples obtained using DMA.

Sample	$T_{g1}$ (°C)	$T_{g2}$ (°C)
CS <sub>60</sub>	30	123
CS <sub>60</sub> /SiO <sub>2</sub> -2.5	50	129
CS <sub>60</sub> /SiO <sub>2</sub> -4.5	52	132
CS <sub>60</sub> /SiO <sub>2</sub> -6.5	62	135

A single endothermic peak in the range of 75–150 °C can be seen in DSC curves, as shown in Figure 5f, corresponding to non-freezing water locked in the amorphous region of the chitosan matrix [67]. Both amino and carboxyl groups can easily bind to water molecules in chitosan, and the water bound by the amino group evaporated faster than that held by carboxyl groups [65]. After the addition of hydrophilic nano-SiO<sub>2</sub> containing a large number of hydroxyl groups, the water locked in the matrix evaporated more slowly, which explains the increase in the endothermic peak.

### 3.4. Water Vapor Permeability

The WVP of the film determines the water transfer between the surrounding atmosphere and the packaging environment. The permeability of a thin film largely depends on its chemical structure, morphology, and hydrophilicity. Figure 6a shows the water vapor transmittance of CS<sub>60</sub> and CS/sorbitol/SiO<sub>2</sub> composite films. The WVP of a CS<sub>60</sub> composite film ( $10.22 \times 10^{-12}$  g·cm/cm<sup>2</sup>·s·Pa) without the addition of nano-SiO<sub>2</sub> is significantly higher than CS<sub>60</sub>/SiO<sub>2</sub>-2.5 ( $7.475 \times 10^{-12}$  g·cm/cm<sup>2</sup>·s·Pa), CS<sub>60</sub>/SiO<sub>2</sub>-4.5 ( $5.048 \times 10^{-12}$  g·cm/cm<sup>2</sup>·s·Pa) and CS<sub>60</sub>/SiO<sub>2</sub>-6.5 ( $6.096 \times 10^{-12}$  g·cm/cm<sup>2</sup>·s·Pa). The overall trend and magnitude of WVP in the film samples are similar to the results of Dong et al. [48,68,69]. The composite film with added nanoparticles has a significantly higher moisture resistance than CS<sub>60</sub>. With the addition of nano-SiO<sub>2</sub> (when the amount of nano-SiO<sub>2</sub> is less than 6.5 wt %), the WVP of CS/sorbitol/SiO<sub>2</sub> composite films gradually decreases, and a dense network structure is formed by secondary bonds, possibly due to the good dispersion of nano-SiO<sub>2</sub> within chitosan molecules and good compatibility of each component [48]. In addition, due to the hydrogen bonding between nano-SiO<sub>2</sub> and CS, as well as the uniformly distributed impermeable nano-particle layer, water vapor is forced to pass through the film through a more tortuous path, thereby increasing the effective path length for the diffusion and improvements in the WVP of the chitosan composite film [57,60,70]. Adding 6.5 wt % of nano-SiO<sub>2</sub>, an excessive amount, results in a large number of hydroxyl groups forming on the surface of nano-SiO<sub>2</sub>, which has high surface energy and is prone to uneven dispersion and aggregation (as shown in Figure 3i), resulting in a discontinuous structure with chitosan molecules. Water molecules are more likely to pass through, resulting in an increase in the moisture permeability coefficient.

### 3.5. Water Contact Angle

The surface water contact angle is an important parameter reflecting the wetting characteristics of film materials. When a droplet forms on a solid surface, wetting occurs. The droplet first contacts the substrate, forming a solid–liquid–gas three-phase contact line. Then, the three-phase contact line continues to move forward and is stable or metastable at a certain radius. The WCA values of chitosan composite films without nano-SiO<sub>2</sub> and with different amounts of nano-SiO<sub>2</sub> are shown in Figure 6b. The WCA value of the CS<sub>60</sub> film is  $72.6 \pm 0.83^\circ$ , which is higher than that of the chitosan composite film containing nano-SiO<sub>2</sub>: CS<sub>60</sub>/SiO<sub>2</sub>-2.5 ( $60.5 \pm 0.54^\circ$ ), CS<sub>60</sub>/SiO<sub>2</sub>-4.5 ( $53.8 \pm 0.75^\circ$ ), CS<sub>60</sub>/SiO<sub>2</sub>-6.5 ( $44.6 \pm 0.69^\circ$ ).

The presence of silica particles reduces the WCA of the film, indicating that the addition of SiO<sub>2</sub> reduces the surface hydrophobicity of the chitosan composite film. This is due to the large number of hydroxyl groups and high hydrophilicity of SiO<sub>2</sub> nanoparticles on the surface of the composite film, which occupy a considerable area (as shown in Figure 3). When water droplets come into contact with the film, they quickly diffuse due to the attraction of hydroxyl groups [57,71]. Martínez-Aguilar et al. [72] added nano-SiO<sub>2</sub>

to a PLA film, observing that the WCA of the film decreased. Yu et al. [71] constructed a superhydrophilic surface with nano-SiO<sub>2</sub> on chitosan film; the WCA of the film decreased from 66.1° to 3°. They both emphasized the importance of hydroxyl groups in nano-SiO<sub>2</sub>.

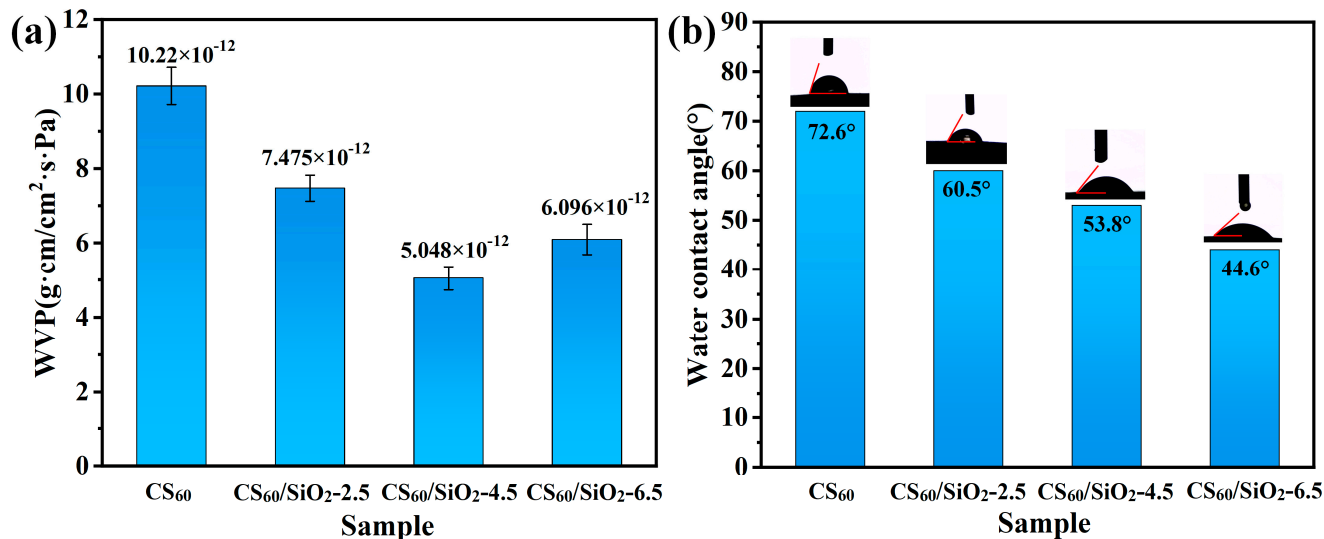


Figure 6. (a) WVP and (b) WCA of chitosan-based composite films.

#### 4. Conclusions

The chitosan-based nanocomposite films were prepared with sorbitol as a plasticizer and nano-SiO<sub>2</sub> as the reinforcing agent via the solvent casting method, assisted by ultrasonication. The sorbitol showed a good plasticizing effect on pure chitosan film while the elongation at break of CS<sub>75</sub> increased from 5.9% to >80%. The CS<sub>60</sub> with the best toughness was selected as the subsequent nanocomposite's matrix. When mixed with nano-SiO<sub>2</sub>, the WVP and thermal stability of the chitosan film both improved while the WCA of the film decreased, turning the film into hydrophilic material. Furthermore, strong hydrogen bonds between nano-SiO<sub>2</sub> and chitosan could reduce the crystallinity of the film. The CS<sub>60</sub>/SiO<sub>2</sub>-4.5 presented excellent physicochemical properties, with the largest elongation at break of 90.8% (14 times that of pure chitosan) and toughness of 10.52 MJm<sup>-3</sup> (6 times that of pure chitosan). This paper has good practical guiding significance for broadening the application of chitosan composite films and the industrial production of biomass plastics.

**Author Contributions:** W.Z. (Wei Zhang): conceptualization, investigation, data curation, validation, formal analysis, writing—original draft, writing—review and editing, visualization. W.Z. (Wentao Zhou): investigation, data curation. Z.Z.: investigation. D.Z.: project administration. Z.G.: formal analysis. P.R.: conceptualization. F.L.: funding acquisition, conceptualization. All authors have read and agreed to the published version of the manuscript.

**Funding:** The authors gratefully acknowledge the National Natural Science Foundation of China (Grant Nos. 52102303 and 52103095), and the and the Xi'an Science and Technology Plan Project (Grant Nos. 22GXFW0092 and 22GXFW0097). The authors also thank the shiyanjia lab ([www.Shiyanjia.com](http://www.Shiyanjia.com)) (accessed on 15 August 2023) for the SEM test.

**Institutional Review Board Statement:** Not applicable.

**Informed Consent Statement:** Not applicable.

**Data Availability Statement:** The authors do not have permission to share data.

**Conflicts of Interest:** The authors declare that they have no known competing financial interests or personal relationships that could have appeared to influence the work reported in this paper.

## References

1. Ncnbe, L.K.; Ude, A.U.; Ogunmuyiwa, E.N.; Zulkifli, R.; Beas, I.N. Environmental Impact of Food Packaging Materials: A Review of Contemporary Development from Conventional Plastics to Polylactic Acid Based Materials. *Materials* **2020**, *13*, 4994.
2. Liu, M.; Zhou, Y.; Zhang, Y.; Yu, C.; Cao, S. Preparation and structural analysis of chitosan films with and without sorbitol. *Food Hydrocoll.* **2013**, *33*, 186–191. [[CrossRef](#)]
3. Salama, A.; Hesemann, P. New N-guanidinium chitosan/silica ionic microhybrids as efficient adsorbent for dye removal from waste water. *Int. J. Biol. Macromol.* **2018**, *111*, 762–768. [[CrossRef](#)] [[PubMed](#)]
4. Yang, H.; Liu, Z.; Yin, C.; Han, Z.; Guan, Q.; Zhao, Y.; Ling, Z.; Liu, H.; Yang, K.; Sun, W.; et al. Edible, Ultrastrong, and Microplastic-Free Bacterial Cellulose-Based Straws by Biosynthesis. *Adv. Funct. Mater.* **2021**, *32*, 2111713. [[CrossRef](#)]
5. Bakshi, P.S.; Selvakumar, D.; Kadirvelu, K.; Kumar, N.S. Chitosan as an environment friendly biomaterial—A review on recent modifications and applications. *Int. J. Biol. Macromol.* **2020**, *150*, 1072–1083. [[CrossRef](#)]
6. Wahba, M.I. Enhancement of the mechanical properties of chitosan. *J. Biomater. Sci.-Polym. Ed.* **2019**, *31*, 350–375. [[CrossRef](#)]
7. Melro, E.; Antunes, F.E.; Silva, G.J.; Cruz, I.; Ramos, P.E.; Carvalho, F.; Alves, L. Chitosan Films in Food Applications. Tuning Film Properties by Changing Acidic Dissolution Conditions. *Polymers* **2021**, *13*, 1. [[CrossRef](#)]
8. El-banna, F.S.; Mahfouz, M.E.; Leporatti, S.; El-Kemary, M.; Hanafy, N.A.N. Chitosan as a Natural Copolymer with Unique Properties for the Development of Hydrogels. *Appl. Sci.* **2019**, *9*, 2193. [[CrossRef](#)]
9. Priyadarshi, R.; Rhim, J.-W. Chitosan-based biodegradable functional films for food packaging Applications. *Innov. Food. Sci. Emerg. Technol.* **2020**, *62*, 10234. [[CrossRef](#)]
10. Sharkawy, A.; Barreiro, M.F.; Rodrigues, A.E. Chitosan-based Pickering emulsions and their applications: A review. *Carbohydr. Polym.* **2020**, *250*, 116885. [[CrossRef](#)]
11. Qiao, H.; Li, L.; Zhou, X.; Gao, X.; Li, X.; Wang, Y.; Zhang, Y.; Liao, Y.; Zhou, X.; Zhou, H.; et al. Efficient preparation of all cellulose composite films using a plasticizing-rolling method. *Compos. Part A* **2022**, *158*, 106968. [[CrossRef](#)]
12. Tan, S.; Andriyana, A.; Ong, H.C.; Lim, S.; Pang, Y.L.; Ngoh, G.C. A Comprehensive Review on the Emerging Roles of Nanofillers and Plasticizers towards Sustainable Starch-Based Bioplastic Fabrication. *Polymers* **2022**, *14*, 664. [[CrossRef](#)] [[PubMed](#)]
13. Luangtana-anan, M.; Soradech, S.; Saengsod, S.; Nunthanid, J.; Limmatvapirat, S. Enhancement of Moisture Protective Properties and Stability of Pectin through Formation of a Composite Film: Effects of Shellac and Plasticizer. *J. Food Sci.* **2017**, *82*, 2915–2925. [[CrossRef](#)] [[PubMed](#)]
14. Ballesteros-Mártinez, L.; Pérez-Cervera, C.; Andrade-Pizarro, R. Effect of glycerol and sorbitol concentrations on mechanical, optical, and barrier properties of sweet potato starch film. *NFS J.* **2020**, *20*, 1–9. [[CrossRef](#)]
15. Farhan, A.; Hani, N.M. Characterization of edible packaging films based on semi-refined kappa-carrageenan plasticized with glycerol and sorbitol. *Food Hydrocoll.* **2017**, *64*, 48–58. [[CrossRef](#)]
16. Hanan, Z.A.N.; Roos, Y.H.; Kerry, J.P. Use and application of gelatin as potential biodegradable packaging materials for food products. *Int. J. Biol. Macromol.* **2014**, *71*, 94–102. [[CrossRef](#)]
17. Thakhiew, W.; Devahastin, S.; Soponronnarit, S. Effects of drying methods and plasticizer concentration on some physical and mechanical properties of edible chitosan films. *J. Food. Eng.* **2010**, *99*, 216–224. [[CrossRef](#)]
18. Leceta, I.; Guerrero, P.; Caba, K. Functional properties of chitosan-based films. *Carbohydr. Polym.* **2013**, *93*, 339–346. [[CrossRef](#)]
19. Mei, J.; Yuan, Y.; Wu, Y.; Li, Y. Characterization of edible starch–chitosan film and its application in the storage of Mongolian cheese. *Int. J. Biol. Macromol.* **2013**, *57*, 17–21. [[CrossRef](#)]
20. Dayarian, S.; Zamani, A.; Moheb, A.; Masoomi, M. Physico-Mechanical Properties of Films of Chitosan, Carboxymethyl Chitosan, and Their Blends. *J. Polym. Environ.* **2014**, *22*, 409–416. [[CrossRef](#)]
21. Amin, K.A.M.; Panhuis, M. Reinforced Materials Based on Chitosan, TiO<sub>2</sub> and Ag Composites. *Polymers* **2012**, *4*, 590–599. [[CrossRef](#)]
22. Budnyak, T.M.; Pylypchuk, I.V.; Tertykh, V.A.; Yanovska, E.S.; Kolodynska, D.K. Synthesis and adsorption properties of chitosan-silica nanocomposite prepared by sol-gel method. *Nanoscale Res. Lett.* **2015**, *10*, 87. [[CrossRef](#)] [[PubMed](#)]
23. Sharififard, H.; Rezvannapanah, E. Ultrasonic-assisted synthesis of SiO<sub>2</sub> nanoparticles and SiO<sub>2</sub>/chitosan/Fe nanocomposite and their application for vanadium adsorption from aqueous solution. *Environ. Sci. Pollut. Res.* **2020**, *28*, 11586–11597. [[CrossRef](#)]
24. Mark, J.E. Some interesting things about polysiloxanes. *Acc. Chem. Res.* **2004**, *37*, 946–953. [[CrossRef](#)] [[PubMed](#)]
25. Chen, Q.; Gong, S.; Moll, J.; Zhao, D.; Kumar, S.K.; Colby, R.H. Mechanical Reinforcement of Polymer Nanocomposites from Percolation of a Nanoparticle Network. *ACS Macro. Lett.* **2015**, *4*, 398–402. [[CrossRef](#)]
26. Li, Z.; Li, H.; Wang, M.; Zhang, Z.; Yang, L.; Ma, L.; Liu, H. Preparation and Properties of Poly(butylene adipate-co-terephthalate)/thermoplastic Hydroxypropyl Starch Composite Films Reinforced with Nano-Silica. *Polymers* **2023**, *15*, 2026. [[CrossRef](#)] [[PubMed](#)]
27. Zhu, J.; Gao, W.; Wang, B.; Kang, X.; Liu, P.; Cui, B.; El-Aty, A.M.A. Preparation and evaluation of starch-based extrusion-blown nanocomposite films incorporated with nano-ZnO and nano-SiO<sub>2</sub>. *Int. J. Biol. Macromol.* **2021**, *183*, 1371–1378. [[CrossRef](#)]
28. Marangoni, L.; Rodrigues, P.R.; Silva, R.G.; Vieira, R.P.; Alves, R.M.V. Improving the mechanical properties and thermal stability of sodium alginate/hydrolyzed collagen films through the incorporation of SiO<sub>2</sub>. *Curr. Res. Food Sci.* **2022**, *5*, 96–101. [[CrossRef](#)]
29. ASTM D638:2022; Standard Test Method for Tensile Properties of Plastics. ASTM: Conshohocken, PA, USA, 2022.
30. Badawy, M.E.I. A new rapid and sensitive spectrophotometric method for determination of a biopolymer chitosan. *Int. J. Carbohydr. Chem.* **2012**, *2012*, 139328. [[CrossRef](#)]

31. Lim, S.H.; Hudson, S.M. Synthesis and antimicrobial activity of a water-soluble chitosan derivative with a fiber-reactive group. *Carbohydr. Res.* **2004**, *339*, 313–321. [[CrossRef](#)]
32. Gu, W.; Wu, P. FT-IR and 2D-IR spectroscopic studies on the effect of ions on the phase separation behavior of PVME aqueous solution. *Anal. Sci.* **2007**, *23*, 823. [[CrossRef](#)] [[PubMed](#)]
33. Piermaria, J.; Bosch, A.; Pinoti, A.; Yantorno, O.; Garcia, M.A.; Abraham, A.G. Kefiran films plasticized with sugars and polyols; water vapor barrier and mechanical properties in relation to their microstructure analyzed by ATRFTIR spectroscopy. *Food Hydrocol.* **2011**, *25*, 1261–1269. [[CrossRef](#)]
34. Zhao, Y.; Wei, B.; Wu, M.; Zhang, H.; Yao, J.; Chen, X.; Shao, Z. Preparation and characterization of antibacterial poly(lactic acid)nanocomposites with N-halamine modified silica. *Int. J. Biol. Macromol.* **2020**, *155*, 1468–1477. [[CrossRef](#)] [[PubMed](#)]
35. Hou, J.; Yan, X. Preparation of chitosan-SiO<sub>2</sub> nanoparticles by ultrasonic treatment and its effect on the properties of starch film. *Int. J. Biol. Macromol.* **2021**, *189*, 271–278. [[CrossRef](#)]
36. Zhong, T.; Xia, M.; Yao, Z.; Han, C. Chitosan/Silica Nanocomposite Preparation from Shrimp Shell and Its Adsorption Performance for Methylene Blue. *Sustainability* **2023**, *15*, 47. [[CrossRef](#)]
37. Ali, F.; Khan, S.B.; Kamal, T.; Alamry, K.A.; Bakhsh, E.M.; Asiri, A.M.; Sobahi, T.R.A. Synthesis and characterization of metal nanoparticles templated chitosan-SiO<sub>2</sub> catalyst for the reduction of nitrophenols and dyes. *Carbohydr. Polym.* **2018**, *192*, 217–230. [[CrossRef](#)]
38. Song, X.; Liu, L.; Wu, X.; Liu, Y.; Yuan, J. Chitosan-Based Functional Films Integrated with Magnolol: Characterization, Antioxidant and Antimicrobial Activity and Pork Preservation. *Int. J. Mol. Sci.* **2021**, *22*, 7769. [[CrossRef](#)]
39. Qiao, C.; Ma, X.; Zhang, J.; Yao, J. Molecular interactions in gelatin/chitosan composite films. *Food. Chem.* **2017**, *235*, 45–50. [[CrossRef](#)]
40. Ogawa, K.; Yui, T.; Okuyama, K. Three D structures of chitosan. *Int. J. Biol. Macromol.* **2004**, *34*, 1–8. [[CrossRef](#)]
41. Niu, N.; Teng, S.; Zhou, H.; Qian, H. Synthesis, Characterization, and In Vitro Drug Delivery of Chitosan-Silica Hybrid Microspheres for Bone Tissue Engineering. *J. Nanomater.* **2019**, *2019*, 7425787. [[CrossRef](#)]
42. Montoille, L.; Vicencio, C.M.; Fontalba, D.; Ortiz, J.A.; Moreno-Serna, V.; Peponi, L.; Matiacevich, S.; Zapata, P.A. Study of the effect of the addition of plasticizers on the physical properties of biodegradable films based on kefirin for potential application as food packaging. *Food. Chem.* **2021**, *360*, 129966. [[CrossRef](#)] [[PubMed](#)]
43. Ghasemlou, M.; Khodaiyan, F.; Oromiehie, A. Rheological and structural characterisation of film-forming solutions and biodegradable edible film made from kefirin as affected by various plasticizer types. *Int. J. Biol. Macromol.* **2011**, *49*, 814–821. [[CrossRef](#)] [[PubMed](#)]
44. Hazrati, K.Z.; Sapuan, S.M.; Zuhri, M.Y.M.; Jumaidin, R. Effect of plasticizers on physical, thermal, and tensile properties of thermoplastic films based on Dioscorea hispida starch. *Int. J. Biol. Macromol.* **2021**, *185*, 219–228. [[CrossRef](#)] [[PubMed](#)]
45. Ma, X.; Qiao, C.; Zhang, J.; Xu, J. Effect of sorbitol content on microstructure and thermal properties of chitosan films. *Int. J. Biol. Macromol.* **2018**, *119*, 1294–1297. [[CrossRef](#)] [[PubMed](#)]
46. Dong, W.; Su, J.; Chen, Y.; Xu, D.; Cheng, L.; Mao, L.; Gao, Y.; Yuan, F. Characterization and antioxidant properties of chitosan film incorporated with modified silica nanoparticles as an active food packaging. *Food Chem.* **2022**, *373*, 131414. [[CrossRef](#)]
47. Boughriba, S.; Souissi, N.; Jridi, M.; Li, S.; Nasri, M. Thermal, mechanical and microstructural characterization and antioxidant potential of Rhinobatos cemiculus gelatin films supplemented by titanium dioxide doped silver nanoparticles. *Food Hydrocol.* **2020**, *103*, 105695. [[CrossRef](#)]
48. Dong, Z.; Qiao, Y.; Yu, M.; Zhang, X.; Wnag, J.; Hu, S.; Zhai, K. Preparation and Performances of Starch/Chitosan/Nano Silica Composite Packaging Film. *China Plast. Ind.* **2017**, *45*, 135–139.
49. Hosseini, S.; Rezaei, M.; Zandi, M.; Farahmandghavi, F. Fabrication of bio-nanocomposite films based on fish gelatin reinforced with chitosan nanoparticles. *Food Hydrocol.* **2015**, *44*, 172–182. [[CrossRef](#)]
50. Chang, P.R.; Jian, R.; Yu, J.; Ma, X. Fabrication and characterisation of chitosan nanoparticles/plasticised-starch composites. *Food Chem.* **2010**, *120*, 136–740. [[CrossRef](#)]
51. Sun, Y.; Liu, Z.; Zhang, L.; Wang, X.; Li, L. Effects of plasticizer type and concentration on rheological, physico-mechanical and structural properties of chitosan/zein film. *Int. J. Biol. Macromol.* **2020**, *143*, 334–340. [[CrossRef](#)]
52. Liu, M.; Mao, Z.; Jiang, X.; Yu, C.; Niu, Y.; Zhou, Y. Properties of Chitosan Film-Forming Solution and Its Films. *Food. Sci.* **2014**, *35*, 11–15.
53. Galus, S.; Gaouditz, M.; Kowalska, H.; Debeaufort, F. Effects of Candelilla and Carnuba Wax Incorporation on the Functional Properties of Edible Sodium Caseinate Films. *Int. J. Mol. Sci.* **2020**, *21*, 9349. [[CrossRef](#)] [[PubMed](#)]
54. Peng, Y.; Yin, L.; Li, Y. Combined effects of lemon essential oil and surfactants on physical and structural properties of chitosan films. *Int. J. Food Sci. Technol.* **2012**, *48*, 44–50. [[CrossRef](#)]
55. Hou, X.; Xue, Z.; Xia, Y.; Qin, Y.; Zhang, G.; Liu, H.; Li, K. Effect of SiO<sub>2</sub> nanoparticle on the physical and chemical properties of eco-friendly agar/sodium alginate nanocomposite film. *Int. J. Biol. Macromol.* **2019**, *125*, 1289–1298. [[CrossRef](#)] [[PubMed](#)]
56. Peighambardoust, S.J.; Peighambardoust, S.H.; Pournasir, N.; Pakdel, P.M. Properties of active starch-based films incorporating a combination of Ag, ZnO and CuO nanoparticles for potential use in food packaging application. *Food Packag. Shelf Life* **2020**, *22*, 100420. [[CrossRef](#)]
57. Oliveira, F.; Barros-Timmons, A.; Lopes-da-Silva, J.A. Preparation and Characterization of Chitosan/SiO<sub>2</sub> Composite Films. *J. Nanosci. Nanotechnol.* **2010**, *10*, 2816–2825. [[CrossRef](#)]

58. Zhai, X.; Zou, X.; Shi, J.; Huang, X.; Sun, Z.; Li, Z.; Sun, Y.; Li, Y.; Wang, X.; Holmes, M.; et al. Amine-responsive bilayer films with improved illumination stability and electrochemical writing property for visual monitoring of meat spoilage. *Sens. Actuators B Chem.* **2020**, *302*, 127130. [[CrossRef](#)]
59. Chen, X.; Sun, L.; Wang, H.; Cao, S.; Shang, T.; Yan, H.; Lin, Q. Nano-SiO<sub>2</sub> reinforced alginate-chitosan-gelatin nanocomposite hydrogels with improved physicochemical properties and biological activity. *Colloids Surf. B* **2023**, *228*, 13413. [[CrossRef](#)]
60. Liu, M.; Zhou, Y.; Zhang, Y.; Yu, C.; Cao, S. Physicochemical, mechanical and thermal properties of chitosan films with and without sorbitol. *Int. J. Biol. Macromol.* **2014**, *70*, 340–346. [[CrossRef](#)]
61. Martínez-Camacho, A.P.; Cortez-Rocha, M.O.; Ezquerro-Brauer, J.M.; Graciano-Verdugo, A.Z.; Rodriguez-Félix, F.; Castillo-Ortega, M.M.; Yépiz-Gómez, M.S.; Plascencia-Jatomea, M. Chitosan composite films: Thermal, structural, mechanical and antifungal properties. *Carbohydr. Polym.* **2010**, *82*, 305–315. [[CrossRef](#)]
62. Liu, M.; Dai, L.; Shi, H.; Xiong, S.; Zhou, C. In vitro evaluation of alginate/halloysite nanotube composite scaffolds for tissue engineering. *Mater. Sci. Eng. C* **2015**, *49*, 700–712. [[CrossRef](#)] [[PubMed](#)]
63. Rafiq, S.; Heydarinasab, A. Mesoporous Chitosan-SiO<sub>2</sub> Nanoparticles: Synthesis, characterization and CO<sub>2</sub> adsorption capacity. *ACS Sustain. Chem. Eng.* **2017**, *5*, 10379–10386. [[CrossRef](#)]
64. Qiao, C.; Ma, X.; Wang, X.; Liu, L. Structure and properties of chitosan films: Effect of the type of solvent acid. *LWT-Food Sci. Technol.* **2021**, *135*, 109984. [[CrossRef](#)]
65. Iturraga, L.; Olabarrieta, I.; Castellán, A.; Gardrat, C.; Coma, V. Active naringin-chitosan films: Impact of UV irradiation. *Carbohydr. Polym.* **2014**, *110*, 374–381. [[CrossRef](#)]
66. Liu, M.; Zhang, Y.; Wu, C.; Xiong, S.; Zhou, C. Chitosan/halloysite nanotubes bionanocomposites: Structure, mechanical properties and biocompatibility. *Int. J. Biol. Macromol.* **2012**, *51*, 566–575. [[CrossRef](#)]
67. Ghosa, A.; Ali, M.A.; Walls, R. Modification of microstructural morphology and physical performance of chitosan films. *Int. J. Biol. Macromol.* **2010**, *46*, 179–186. [[CrossRef](#)]
68. Li, W.; Zheng, K.; Chen, H.; Feng, S.; Wang, W.; Qin, C. Influence of Nano Titanium Dioxide and Clove Oil on Chitosan-Starch Film Characteristics. *Polymers* **2019**, *11*, 1418. [[CrossRef](#)]
69. Hussein, E.M.; Desoky, W.M.; Hanafy, M.F.; Guirguis, O.W. Effect of TiO<sub>2</sub> nanoparticles on the structural configurations and thermal, mechanical, and optical properties of chitosan/TiO<sub>2</sub> nanoparticle composites. *J. Phys. Chem. Solids* **2021**, *152*, 109983. [[CrossRef](#)]
70. Roy, S.; Rhim, J.-W.; Jaiswal, L. Bioactive agar-based functional composite film incorporated with copper sulfide nanoparticles. *Food Hydrocoll.* **2019**, *93*, 156–166. [[CrossRef](#)]
71. Yu, M.; Zhao, S.; Yang, L.; Ji, N.; Wang, Y.; Xiong, L.; Sun, Q. Preparation of a superhydrophilic SiO<sub>2</sub> nanoparticles coated chitosan-sodium phytate film by a simple ethanol soaking process. *Carbohydr. Polym.* **2021**, *271*, 118422. [[CrossRef](#)]
72. Martínez-Aguilar, V.; Peña-Juarez, M.G.; Carrillo-Sánchez, P.C.; López-Zamora, L.; Delgado-Alvarado, E.; Gutiérrez-Castaneda, E.J.; Flores-Martínez, N.L.; Herrera-May, A.L.; González-Calderón, J.A. Evaluation of the Antioxidant and Antimicrobial Potential of SiO<sub>2</sub> Modified with Cinnamon Essential Oil (*Cinnamomum verum*) for Its Use as a Nanofiller in Active Packaging PLA Films. *Antioxidants* **2023**, *12*, 1090. [[CrossRef](#)] [[PubMed](#)]

**Disclaimer/Publisher's Note:** The statements, opinions and data contained in all publications are solely those of the individual author(s) and contributor(s) and not of MDPI and/or the editor(s). MDPI and/or the editor(s) disclaim responsibility for any injury to people or property resulting from any ideas, methods, instructions or products referred to in the content.